Structure
Article

Structure of Hydrogenase Maturation Protein HypF with Reaction Intermediates Shows Two Active Sites

Svetlana Petkun,[1] Rong Shi,[1] Yunge Li,[2] Abdalin Asinas,[1] Christine Munger,[1] Linhua Zhang,[1] Mandy Waclawek,[3] Basem Soboh,[3] R. Gary Sawers,[3] and Miroslaw Cygler[1,2,4,*]
[1]Department of Biochemistry, McGill University, Montreal, QC H3G 1Y6, Canada
[2]Biotechnology Research Institute, National Research Council, Montreal, QC H4P 2R2, Canada
[3]Department of Microbiology, Martin Luther University Halle-Wittenberg, 06120 Halle, Germany
[4]Present address: Department of Biochemistry, University of Saskatchewan, Saskatoon, SK S7N 5E5, Canada
*Correspondence: miroslaw.cygler@usask.ca
DOI 10.1016/j.str.2011.09.023

SUMMARY

[NiFe]-hydrogenases are multimeric proteins. The large subunit contains the $NiFe(CN)_2CO$ bimetallic active center and the small subunit contains Fe-S clusters. Biosynthesis and assembly of the $NiFe(CN)_2CO$ active center requires six Hyp accessory proteins. The synthesis of the CN^- ligands is catalyzed by the combined actions of HypF and HypE using carbamoylphosphate as a substrate. We report the structure of *Escherichia coli* HypF(92–750) lacking the N-terminal acylphosphatase domain. HypF(92–750) comprises the novel Zn-finger domain, the nucleotide-binding YrdC-like domain, and the Kae1-like universal domain, also binding a nucleotide and a Zn^{2+} ion. The two nucleotide-binding sites are sequestered in an internal cavity, facing each other and separated by ~14 Å. The YrdC-like domain converts carbamoyl moiety to a carbamoyl adenylate intermediate, which is channeled to the Kae1-like domain. Mutations within either nucleotide-binding site compromise hydrogenase maturation but do not affect the carbamoylphosphate phosphatase activity.

INTRODUCTION

Hydrogenases are key enzymes involved in hydrogen metabolism, catalyzing the reversible oxidation of molecular hydrogen into protons and electrons. These enzymes are widely distributed in Bacteria and Archaea, and a few are also present in lower Eukarya (Vignais and Billoud, 2007). Hydrogenases consist of three phylogenetically distinct classes: [FeFe]-hydrogenases, [NiFe]-hydrogenases, and [Fe]-hydrogenases (Thauer et al., 2010). The model organism *Escherichia coli* synthesizes three membrane-associated [NiFe]-hydrogenases (Hyd) during anaerobic growth (Forzi and Sawers, 2007). Whereas Hyd-1 and Hyd-2 are hydrogen-oxidizing enzymes, Hyd-3 together with the formate dehydrogenase H forms the hydrogen-evolving formate hydrogenlyase complex.

Structural studies on the [NiFe]-hydrogenases and [FeFe]-hydrogenases showed that they display significant similarities in their structural framework and chemistry, despite the absence of any resemblance between the folds surrounding them (Peters et al., 1998; Volbeda et al., 1995). They comprise multisubunit complexes in which the large subunit contains the reaction center involving Ni and/or Fe ions, whereas the small subunit harbors the Fe-S clusters that participate in an electron relay from the active site to the redox partner (Vignais and Billoud, 2007).

The active sites of both [NiFe]-hydrogenases and [FeFe]-hydrogenases have carbon monoxide and cyanide ligands coordinated to the iron atoms. Despite this instance of convergent evolution, apparently quite distinct metabolic intermediates, enzyme mechanisms, and sets of proteins are employed to synthesize and insert these diatomic ligands into the different hydrogenases (Böck et al., 2006; Mulder et al., 2010). Although considerable progress has been achieved in identifying key steps in the biosynthesis of both sets of active sites, a number of important questions, such as how the specific metal is inserted into the target protein, how correct folding of the precursor of the enzyme for the insertion process is maintained, what governs synthesis of the toxic CN^- and CO ligands, and how the conformational change to achieve the functional metal center is accomplished, remain to be resolved.

Six proteins, conserved in all microorganisms that synthesize [NiFe]-hydrogenases, have been shown to participate in the process of hydrogenase maturation: HypA, HypB, HypC, HypD, HypE, and HypF. HypA and HypB were shown to be involved in Ni insertion (Blokesch et al., 2004a; Mehta et al., 2003), and this process occurs subsequent to insertion of the iron center (Böck et al., 2006). HypE, HypF, HypC, and HypD participate in synthesis and insertion of the $Fe(CN)_2CO$ center. HypE and HypF are specifically involved in the synthesis of the CN^- ligands. HypF has a carbamoyltransferase activity, and it has been proposed (Reissmann et al., 2003) that carbamoyl-AMP, derived from carbamoylphosphate and ATP, acts as an intermediate in the transfer of the carbamoyl moiety to the C-terminal cysteinyl residue of HypE. HypE then catalyzes the ATP-dependent dehydration of the thiocarboxamide to produce a thiocyanate (Blokesch et al., 2004b; Reissmann et al., 2003). The subsequent transfer of the cyano group to the iron to form the metal center is thought to occur on the HypC-HypD complex, but the mechanism requires further elucidation (Böck et al., 2006; Forzi and Sawers, 2007). Nothing is known about how the CO group is generated or introduced onto the iron atom for [NiFe]-hydrogenases.

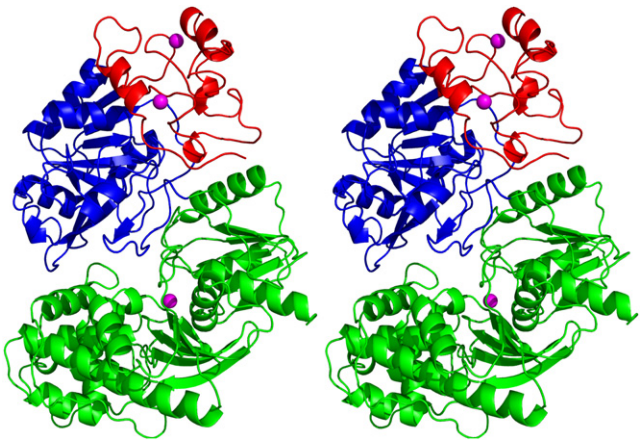

Figure 1. Ribbon Representation of *E. coli* HypF(92–750)
The Zn-finger domain is colored red, the middle domain is colored blue, and the C-terminal domain is colored green. Zn atoms are colored magenta.

HypF has an N-terminal acylphosphatase domain (amino acids 1–91), and in the absence of any other substrate HypF dephosphorylates carbamoylphosphate (Paschos et al., 2002). Adjacent to the acylphosphatase domain are two signature zinc-finger motifs (residues 109–184), and toward the C terminus of the protein (residues 473–479) there is a motif characteristic of carbamoyltransferases (Paschos et al., 2002). HypF also catalyzes the carbamoylphosphate-dependent hydrolysis of ATP to AMP and pyrophosphate, and it is unclear whether a carbamoyl-adenylate or carbamoyl-ADP intermediate is involved in the transfer to HypE (Blokesch et al., 2004b; Reissmann et al., 2003).

Structural information for HypC, HypD, and HypE proteins from different organisms has been obtained (Gasper et al., 2006; Rangarajan et al., 2008; Shomura et al., 2007; Wang et al., 2007; Watanabe et al., 2007, 2009; Xia et al., 2009). However, although the structure of the N-terminal acylphosphatase domain of HypF has been determined (Rosano et al., 2002), no other structural information for the HypF protein is available.

In this work, we present the crystal structure of the carbamoyltransferase HypF, which reveals a novel Zn-finger motif, and the presence of two nucleotide-binding domains with ancient folds. The structure combined with mutagenesis and activity measurements enabled us to provide new mechanistic insight into the catalytic function of the enzyme.

RESULTS

Structural Characterization of *E. coli* HypF(92–750)

Efforts to crystallize the full-length HypF protein have yielded no crystals so far. However, the construct containing residues 92–750, in which the N-terminal acylphosphatase domain with already known structure (Rosano et al., 2002) was deleted, could be crystallized. The initial crystals diffracted to low resolution. Mutation to alanines of three consecutive glutamines, predicted to be surface exposed, to reduce surface entropy (Cooper et al., 2007) resulted in a protein variant HypF(92–750)M3 that led to crystals diffracting to 2.0 Å resolution, albeit crystallized under different conditions.

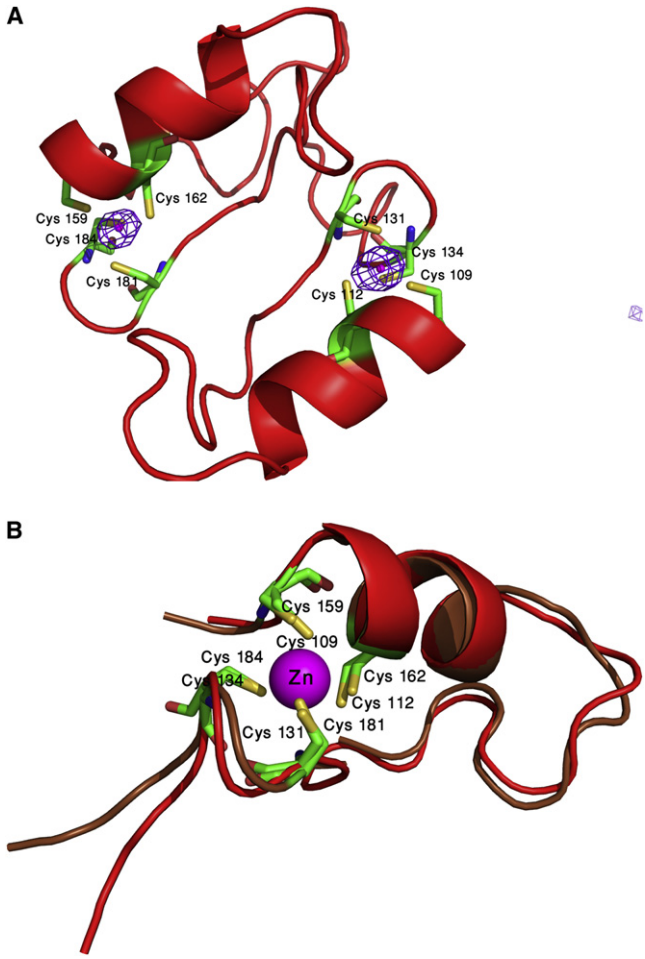

Figure 2. Two Zn Fingers Shown in Cartoon Representation
(A) Anomalous map calculated with the data collected at the Zn absorption edge peak shown at the 10σ level. The map calculated from data collected at the Fe absorption edge shows only a 3σ peak at one of the metal positions.
(B) Superposition of the two Zn fingers. Coordinating cysteine residues are shown in stick representation.

The HypF(92–750) protein is composed of three domains encompassing residues 101–187, 188–378, and 379–746 (Figure 1).

The Zn-Finger Domain

The first domain contains four CXXC motifs and was predicted to be a Zn-finger domain (Paschos et al., 2002). It can be further divided into two subdomains, 101–141 and 142–187, each carrying two CXXC motifs. Each subdomain contains a hairpin helix-loop-extended strand followed by a loop. The first CXXC motif is located at the beginning of the helix and the second is in the loop that follows the extended section (Figure 2A). These four cysteines are the ligands for a metal ion clearly visible in the electron density map. The Zn-finger structural elements encompass residues 107–136 and 157–186. The first metal is bound by Cys109, Cys112, Cys131, and Cys134, whereas the second metal binds to Cys159, Cys162, Cys181, and Cys184. These two Zn fingers share 12 identical residues, corresponding to 40% sequence identity. Not surprisingly, they superimpose with a low root-mean-square deviation (rmsd) of

0.85 Å (Figure 2B). The two Zn fingers pack side by side in an antiparallel fashion, contacting through their extended strands.

The Middle Domain

The middle domain (residues 188–378) contains an extended mixed 11-stranded β sheet flanked by three α helices on one side and two α helices on the other side. The β sheet is highly curved, with a helical twist of 180° between the first and last strands (Figure 1). The molecular surface of this domain contains a deep and long depression located over the tips of strands β8-β5-β7-β6-β10. This region is lined with arginines, lysines, and a histidine and has a highly positive character. This depression faces the C-terminal domain and is part of a large cavity in the HypF structure.

The C-Terminal Domain

The C-terminal domain (residues 379–746) is folded into a crescent-shaped α/β-layered structure with five successive α-β-α-β-α layers. The first and second α-helical layers each contains two α helices, whereas the last α-helical layer contains a bundle of seven helices. Both β sheets are mixed, with six and five β strands, respectively (Figure 1). The concave side of this domain faces the middle domain and is opposite the positively charged depression in its surface and completes the internal cavity. A large peak in the electron density map was found on the concave side of this domain, octahedrally coordinated by Asp502, Asp727, His475, His479, and two water molecules (Figure 3A).

Substrate- and Metal-Binding Sites

Metal-Binding Sites

In addition to the three metal ions described above (two in the Zn-finger domain and one in the C-terminal domain), a fourth metal was identified between two symmetry-related molecules and coordinated by two backbone carbonyl oxygen atoms, a glutamine side chain, and three water molecules. Because HypF is suspected of potentially binding iron, it was essential to determine the identity of these bound metal ions. Therefore, two data sets were collected from the same crystal, one at the Zn absorption peak wavelength (1.28248 Å) and the other at the Fe peak absorption wavelength (1.73989 Å). The anomalous electron density map was calculated for each data set. The map from the Zn-peak wavelength data showed peaks at the metal positions within the Zn-finger domain with heights of 35σ and 25σ, and in the C-terminal domain a peak of 13.7σ. In the Fe-peak map, the peaks at the metal sites in the Zn-finger domain were lower than 4σ, and in the C-terminal domain the peak height was 4.7σ. Because the f′ and f″ for another possible ion, Mn^{2+}, are similar to those for Fe^{2+} at these wavelengths whereas these values for Mg^{2+} are even smaller, we conclude that the three sites are occupied by Zn^{2+} and no Fe is present in these crystals. No significant peak in either anomalous map was found at the location of the intermolecular ion and, based on the ligand-ion distances of ~2.3–2.4 Å and the presence of Mg^{2+} during crystallization, we conclude that this is indeed an Mg^{2+} ion (Harding, 2006). These four metal ions were present in all determined crystal structures of HypF with reasonable temperature factors.

Nucleotide-Binding Sites

The map calculated with the data collected from crystals soaked with the ATP analog AMP-PNP showed electron density corresponding to a triphosphate nucleotide located in the depression within the middle domain (site 1). Electron density for the entire nucleotide is well defined (Figure 3B). The nucleotide molecule is bound with the adenine in an *anti* conformation and the triphosphate following an S-shaped curve (Figure 3B). The phosphates occupy the most positively charged part of the depression, with the α-phosphate being the most buried. The adenine is located in a mildly hydrophobic environment, sandwiched between the side chain of Leu277 and Pro249, with its N6 atom forming a weak hydrogen bond to the carbonyl O^{Glu296} and the O3 hydroxyl to $NH1^{Arg372}$. The α-phosphate is most tightly bound, with its oxygen atoms hydrogen bonded to NH1 and NH2 of Arg245, NH1 of Arg372, and NH of Ser322. The β- and γ-phosphates form one hydrogen bond each to $NH1^{Arg372}$ and NZ^{Lys243}, respectively (Figure 3B). Thus, Arg372 forms three hydrogen bonds to ATP, Arg245 forms two, and Lys243 forms one. Examination of the molecular surface of the middle domain shows the presence of a tunnel that begins under the α-phosphate and emerges on the other side of this domain covered by the edge of the first Zn finger. The tunnel is wider near the α-phosphate and becomes quite narrow in the middle (Figure 3C).

Unexpectedly, in the crystal soaked with AMP-PNP, we observed an additional large blob of electron density located on the concave surface of the C-terminal domain near the Zn^{2+} ion within the interfacial cavity (site 2). The shape of this density corresponded very well to a molecule of ADP (Figure 3D). We presume that ADP was derived from the breakdown of AMP-PNP, which happens at low pH (Sigma-Aldrich product information sheet). Indeed, when the HypF(92–750) crystal was soaked independently with ADP, we observed electron density corresponding to an ADP molecule at the same place within the C-terminal domain. Interestingly, no ADP was bound in site 1 in the middle domain. The ADP molecule in site 2 is located on top of the large β sheet of the C-terminal domain and extends in an approximately perpendicular direction to the sheet. ADP is firmly bound through the participation of the Zn^2 ion (Figure 3D). One oxygen from the α- and one from the β-phosphate coordinate the Zn^{2+} ion, replacing two waters that liganded the metal in the native structure. In addition, the β-phosphate forms two hydrogen bonds to the NH and carbonyl groups of Ile504, whereas the α-phosphate is hydrogen bonded to NH^{Asp727}, NZ^{Lys402}, and NH^{Gly697} (Figure 3D). The adenine also forms several hydrogen bonds: between the N6 atom and $OE1^{Glu623}$, the N1 atom and $ND2^{Asn701}$, and the O2 atom and $NH1^{Arg596}$.

In order to see whether carbamoylphosphate (CP) binds to HypF(92–750), we soaked the crystals with CP and/or ATP or its derivatives. No CP was visible when only CP was soaked into the crystal. When CP and ATP were soaked simultaneously, we observed electron density in site 1. The density fitted AMP and extended somewhat beyond the phosphate group. The carbamoyl adenylate (CBA) fitted well, whereas the β-phosphate of ADP was less compatible with the density. The carbamoyl adenylate is an anticipated intermediate in the transfer reaction, and our structure supports the proposed chemistry (Reissmann et al., 2003). The carbamoyl adenylate group is located in site 1 (Figure 3E) and makes the following contacts with the HypF molecule: $N6^{CBA}$ with O^{Glu296} 2.8 Å; $O3^{*CBA}$ with $NH2^{Arg372}$

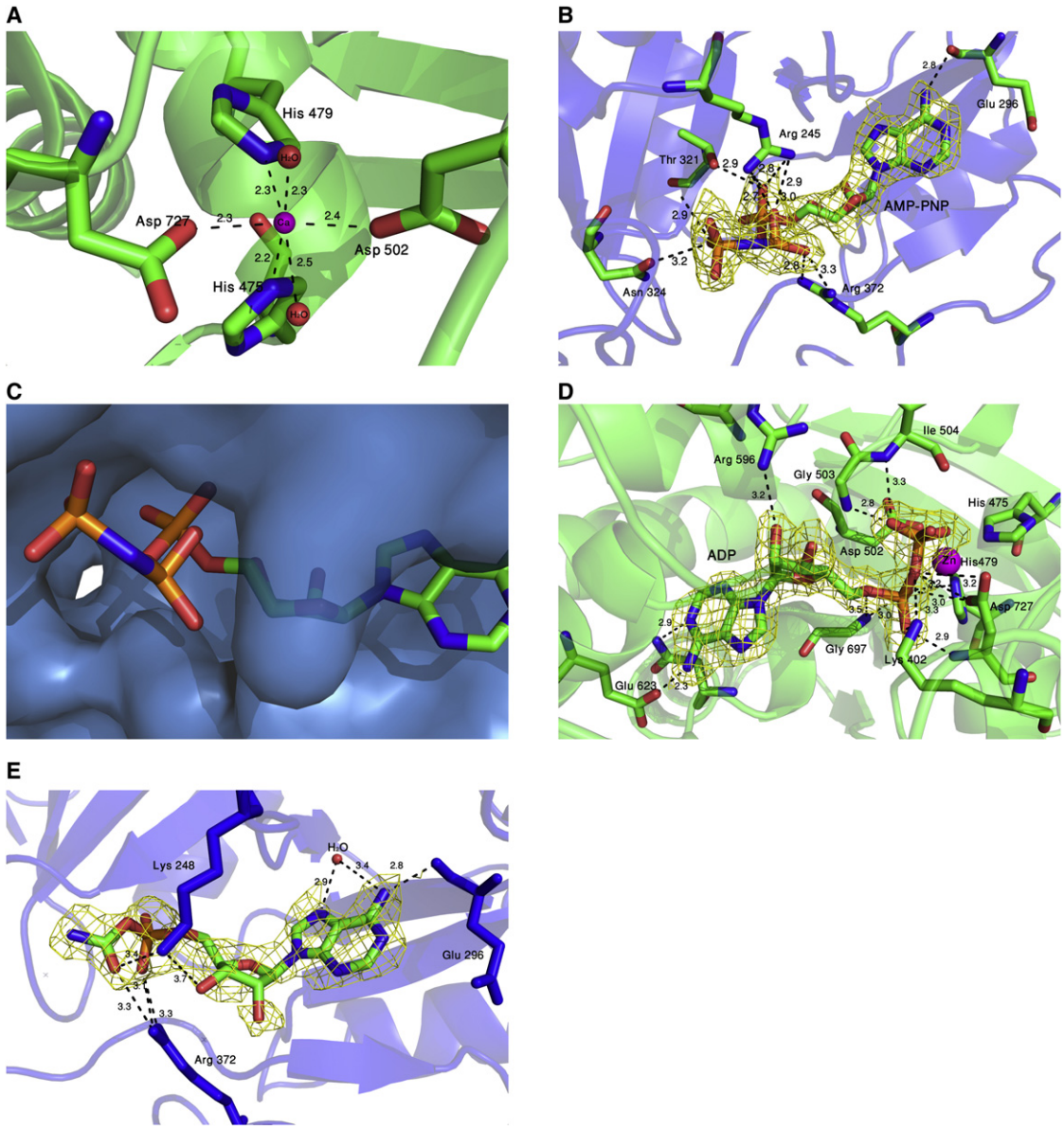

Figure 3. Nucleotide- and Metal-Binding Sites

(A) Coordination of the Zn atom located at the C-terminal domain of HypF. The coordinating residues are shown in stick representation.

(B) AMP-PNP molecule bound at the nucleotide-binding site at the middle domain. Coordinating residues are shown in stick representation. The $2mF_{obs} - DF_{calc}$ electron density for the AMP-PNP molecule is shown contoured at 1.5σ.

(C) A tunnel traversing the middle domain and located near the nucleotide-binding site.

(D) An ADP molecule bound at the C-terminal domain near the Zn ion. The ADP molecule and the coordination residues are shown in stick representation. The $2mF_{obs} - DF_{calc}$ electron density for the ADP molecule contoured at 1.5σ is shown. The Zn^{2+} ion is colored magenta.

(E) The carbamoyl adenylate molecule bound at the nucleotide-binding site at the middle domain. The coordinating residues are shown in stick representation. The $2mF_{obs} - DF_{calc}$ electron density for the carbamoyl adenylate molecule is shown contoured at 1.5σ.

2.8 Å; $O2A^{CBA}$ with $NH1^{Arg372}$ and $NH2^{Arg372}$ 3.1 and 3.0 Å, respectively; and $O1B^{CBA}$ with $NH2^{Arg372}$ 3.3 Å.

Thermodynamics of Nucleotides Binding to HypF

We attempted isothermal titration calorimetry (ITC) experiments with full-length HypF. Unfortunately, due to the tendency of HypF to aggregate, the thermodynamic experiments proved to be impossible. Therefore, the ITC measurements were carried out with the fragment used for crystallization by adding a solution of AMP-PNP, ADP, or carbamoylphosphate to a solution of the HypF(92–750) apoprotein: the occurrence of a binding event was revealed by the presence of exothermic peaks following each addition (Figure 4). Fits of the integrated heat data, carried out using a model involving a single binding event, yielded a K_d of ~6 μM for AMP-PNP and ~4 μM for ADP, and a stoichiometry of 1.2 equivalents of AMP-PNP and 1.02 of ADP per HypF

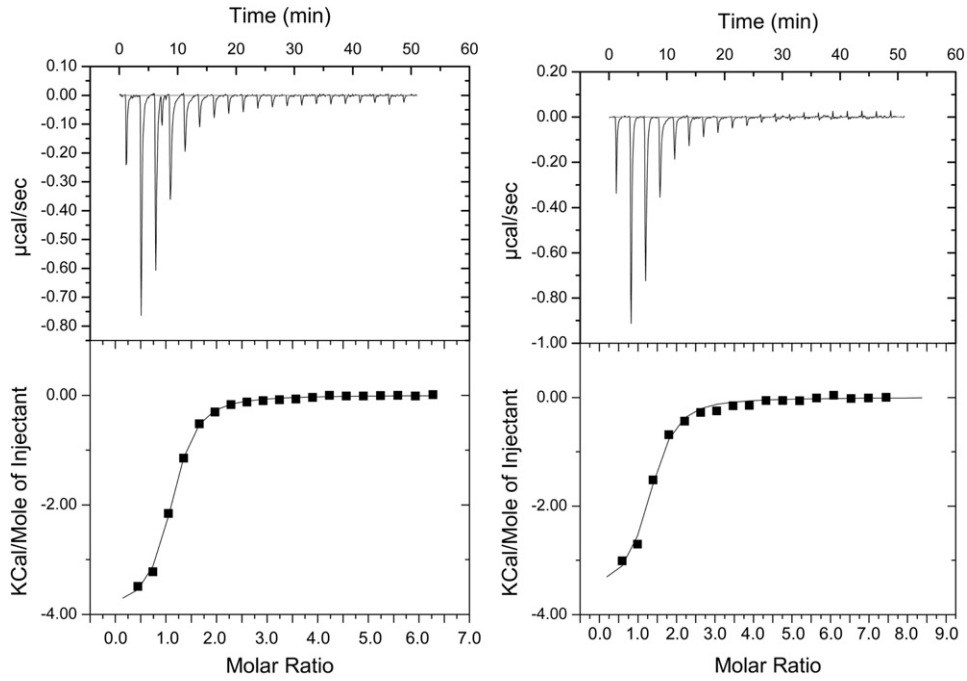

Figure 4. ITC Traces with the Respective Integrated and Normalized Isotherms for HypF(92–750) Titrated with ADP and AMP-PNP
For ADP (left): one-site model, χ^2/df = 1,416, N = 1.02 ± 0.01 sites, K = 2.40*10^5 ± 2.01*10^4 M^{-1}, ΔH = −3,952 ± 61.38 cal/mol, ΔS = 11.1 cal/mol/°. For the AMP-PNP (right): one-site model, χ^2/df = 6,191, N = 1.21 ± 0.04 sites, K = 1.53*10^5 ± 3.18*10^4 M^{-1}, ΔH = −3,601 ± 164.0 cal/mol, ΔS = 11.4 cal/mol/°.

monomer. This process is driven by a large, favorable enthalpic factor (ΔH −3.60 cal mol^{-1} ± 0.16 kcal mol^{-1} in AMP-PNP and ΔH −3.95 cal mol^{-1} ± 0.06 kcal mol^{-1} in the case of ADP) that compensates the positive entropic values (ΔS 11.4 cal mol^{-1} K^{-1} and ΔS 11.1 cal mol^{-1} K^{-1}). No heats were observed during titration with 2 mM carbamoylphosphate.

Mutational Analysis of the Nucleotide-Binding Sites

To determine whether both nucleotide-binding sites identified in the HypF structure are functionally important, we designed amino acid substitutions within nucleotide-binding sites 1 and 2 that introduced either steric hindrance or removed the key interactions and should render the site unavailable for nucleotide binding. Within site 1 (ATP-binding) in the middle domain, we mutated Gly298 to Met. A second double mutant of site 1, Lys243Gln/Arg245Gln, was also generated. Within site 2 (ADP-binding), Gly679 was replaced either by Ala or Val. In the third mutant, both His475 and His479 in site 2 were exchanged for Gln residues. The overall effect of the amino acid alterations on the ability of each of the HypF variants to mature all three hydrogenases was examined by determining the total hydrogenase enzyme activity in crude extracts of the *E. coli hypF* deletion mutant DHP-F2 (Paschos et al., 2002) transformed with plasmids encoding each of the five HypF variants; DHP-F2 is devoid of [NiFe]-hydrogenase activity.

The effect of mutation of site 1 was examined with pFG298M or pFK243Q/R245Q (Table 1). Whereas extracts derived from DHP-F2 transformed with pJW731 encoding wild-type, nonmutated HypF had a hydrogenase enzyme activity of 2.2 U/mg of protein, extracts from DHP-F2 transformed with pFG298M or pFK243Q/R245Q were essentially devoid of hydrogenase activity.

The activities of both hydrogen-oxidizing hydrogenases Hyd-1 and Hyd-2 can be visualized directly after nondenaturing PAGE by staining specifically for hydrogenase enzyme activity (Ballantine and Boxer, 1985). Crude extracts derived from the *E. coli* wild-type strain MC4100 revealed distinct activity bands that correlated with Hyd-1 and Hyd-2 (Figure 5). In contrast, the *hypF* deletion mutant DHP-F2 lacked Hyd-1 and Hyd-2 activity bands, consistent with both enzymes being inactive. Transformation of pJW731 encoding native HypF into strain DHP-F2 restored the hydrogenase activity band pattern observed with MC4100. On the other hand, plasmids pFG298M and pFK243Q/R245Q, when transformed into DHP-F2, failed to restore the Hyd-1 and Hyd-2 activity bands.

The activity of Hyd-3 can also be determined in the direction of proton reduction (dihydrogen evolution) in whole cells by measuring the activity of the formate hydrogenlyase complex using formate as an electron donor (Pinske and Sawers, 2010). Whereas plasmid pJW731 restored wild-type hydrogen evolution activity to DHP-F2, neither strain DHP-F2/pFG298M nor DHP-F2/pFK243Q/R245Q produced hydrogen (Table 1).

Taken together, these results indicate that the activities of Hyd-1, Hyd-2, and Hyd-3 could not be restored by plasmids encoding either HypF variant G298M or HypF variant K243Q/R245Q, strongly suggesting that the amino acid substitutions in nucleotide-binding site 1 abolished HypF maturase activity.

To ensure that the G298M and K243Q/R245Q amino acid substitutions introduced into HypF did not cause destabilization

Table 1. Effects of Amino Acid Substitutions in the ATP-Binding Sites of HypF on Hydrogen Metabolism

Strain	Relative Hydrogenase Activity[a] (U/mg)	Relative Formate Hydrogenlyase Activity[b] (U/mg)
DHP-F2/pJW731	100	100
DHP-F2 (*ΔhypF*)	0.0646 ± 0.0639	<0.01
DHP-F2/pFG697A	16.23 ± 6.53	23.15 ± 0.8
DHP-F2/pFG697V	9.99 ± 2.63	15.9 ± 0.5
DHP-F2/pFG298M	0.045 ± 0.043	<0.01
DHP-F2/pFH475A/H479A	0.0665 ± 0.0345	<0.01
DHP-F2/pFK243Q/R245Q	0.0407 ± 0.0353	<0.01

[a] Total hydrogenase activity was measured as hydrogen-dependent reduction of BV. One hundred percent activity corresponds to a specific activity of 2.87 ± 0.785 μmol H_2 oxidized min^{-1} mg $protein^{-1}$.
[b] Hydrogen evolution activities were measure in whole cells. One hundred percent activity corresponds to a specific activity of 13.6 nmol H_2 evolution min^{-1} mg $protein^{-1}$.

of the enzyme, the HypF protein in extracts of DHP-F2/pJW731, DHP-F2/pFG298M, and DHP-F2/pFK243Q/R245Q was enriched and analyzed by SDS-PAGE (Figure 5). A similar amount of HypF was present in all three extracts.

Nucleotide-binding site 2 in the C-terminal domain of HypF (amino acids 379–746) was probed with three mutants, Gly697Ala, Gly697Val, and His475Gln/His479Gln. Whereas the double-His substitution resulted in a strain unable to synthesize active hydrogenase, the substitutions at Gly697 reduced hydrogenase activity by 85%–90% compared with wild-type HypF (Table 1). Analysis of the level of HypF variants as determined by SDS-PAGE revealed that single-amino acid substitution did not affect HypF stability. In contrast, the double-His substitution variant of HypF could not be detected in extracts of DHP-F2/pFH475Q/H479Q (Figure 6A). Measurement of

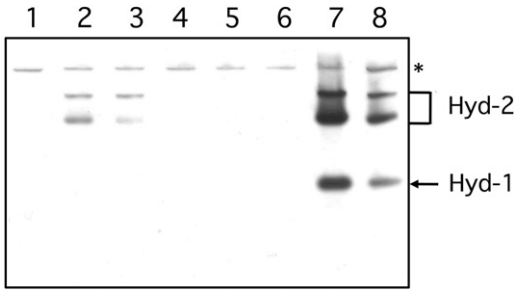

Figure 5. In-Gel Stain for Hydrogenase Enzyme Activity
Proteins in cell extracts (34 μg of protein) derived from DHP-F2 (Δ*hypF*) transformed with plasmids encoding HypF variants were separated by nondenaturing gel electrophoresis (7% [w/v] polyacrylamide) and subsequently stained for hydrogenase activity. The stained bands corresponding to Hyd-1 and Hyd-2 are indicated. Lane 1, DHP-F2 (Δ*hypF*); lane 2, DHP-F2/pFG697A; lane 3, DHP-F2/pFG697V; lane 4; DHP-F2/pFG298M; lane 5, DHP-F2/pFH475A/H479A; lane 6, DHP-F2/pFK243Q/R245Q; lane 7, DHP-F2/pJW731; lane 8, crude extract from MC4100 (wild-type). The weak activity band that migrates at the top of the gel and which is labeled with an asterisk results from a hydrogenase-independent side activity of formate deydrogenase and is not related to the hydrogenases. Nevertheless, it provides a useful loading control.

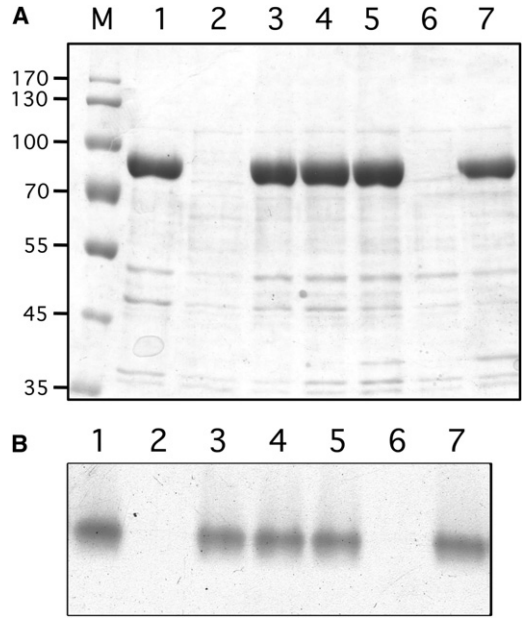

Figure 6. Analysis of the Carbamoylphosphate Phosphatase Activity of Partially Purified HypF ATP-Binding Site Mutants
Equivalent aliquots of enriched HypF variants purified from crude extracts of DHP-F2 (Δ*hypF*) transformed with the plasmids were separated by SDS-PAGE (10% [w/v] polyacrylamide).
(A) Lane M, molecular mass markers indicated in kDa; lane 1, DHP-F2/pJW731 encoding full-length HypF; lane 2, DHP-F2 (Δ*hypF*); lane 3, DHP-F2/pFG697A; lane 4, DHP-F2/pFG697V; lane 5, DHP-F2/pFG298M; lane 6, DHP-F2/pFH475A/H479A; lane 7, DHP-F2/pFK243Q/R245Q. The gel was stained with Coomassie brilliant blue.
(B) A nondenaturing polyacrylamide gel (7% [w/v] polyacrylamide) in which purified HypF variants were separated and the gel was subsequently stained for CP phosphatase activity as described in Experimental Procedures. The lanes are numbered exactly as for (A).

hydrogen evolution in whole cells showed that the Ala-substituted variant of HypF restored 25% of the activity to the Δ*hypF* mutant, whereas the valine-substituted variant restored approximately 15% of the wild-type hydrogen production activity.

In order to determine whether Hyd-1 or Hyd-2 contributed to the total hydrogenase activity measured for the G697 variants of HypF, extracts derived from both strains were analyzed after native PAGE and activity staining (Figure 5). Both plasmids restored weak Hyd-2 activity bands, but essentially no active Hyd-1 enzyme was observed.

Taken together, these data suggest that site 2 is also important for maximal maturation activity of HypF.

Carbamoylphosphate Phosphatase Activity and Hydrogenase Maturation

Previous studies have shown that amino acid substitutions introduced into the acylphosphatase, zinc-finger, or O-carbamoyltransferase (site 2) motifs can lead to abrogation of carbamoylphosphate phosphatase activity as well as defective hydrogenase maturation activity (Paschos et al., 2002). We have shown that functional nucleotide-binding sites are essential for hydrogenase maturation, and we wanted to analyze

whether the same mutations also affected carbamoylphosphate phosphatase activity. The enriched, full-length HypF variants were electrophoretically separated on native PAGE and stained for carbamoylphosphate phosphatase enzyme activity as described in Experimental Procedures. All variants that produced a stable HypF enzyme retained carbamoylphosphate phosphatase activity (Figure 6B).

DISCUSSION

Structural Similarity to Other Proteins

Assembly of functional [NiFe]-hydrogenases requires a set of accessory proteins that deliver the components of the prosthetic groups. These accessory proteins have been widely investigated functionally and structurally (Böck et al., 2006). HypF is the only remaining protein from the [NiFe]-hydrogenase maturation pathway for which no structure was known. We report here the structure of HypF(92–750), which lacks the N-terminal (1–91) acylphosphatase domain. The structure of this small domain was reported previously (Rosano et al., 2002). This domain is linked to the rest of HypF by a flexible linker, thwarting our attempts to crystallize the entire HypF. Moreover, although our construct starts with residue Gln92, the first nine residues are disordered in our structure.

In addition to the N-terminal acylphosphatase domain, the structure of HypF(92–750) reveals that this protein has three additional domains. The first of these is a Zn-finger domain comprising two almost identical Zn fingers, with the Zn^{2+} ions being coordinated by four Cys residues. This domain is essential for HypF function in hydrogenase maturation, shown by a lack of hydrogenase activity in cells expressing HypF cysteine mutants (Paschos et al., 2002). The HypF Zn fingers represent a new topology for a Zn^{2+}-binding domain, as indicated by our search through the Protein Data Bank (PDB) using the Dali server (Holm et al., 2008), which found no structural homologs. The sequences corresponding to these Zn fingers are highly conserved among all known HypF proteins from different species.

The middle domain of HypF shows structural similarity to the YrdC-like proteins, widely distributed in all three domains of life. These domains are found either singly or in conjunction with other domains. The HypF middle domain (amino acids 188–378) overlaps with *E. coli* YrdC (PDB ID code 1HRU; Teplova et al., 2000), *Sulfolobus tokodaii* Sua5 (PDB ID code 2EQA; Agari et al., 2008), and *E. coli* YciO (PDB ID code 1KK9; Jia et al., 2002) with an rmsd of ~1.5–1.6 Å over 120–140 residues. The positively charged depression, which in HypF contains ATP, is conserved in other YrdC-like proteins. Indeed, a nucleotide molecule binds in the same place within the structure of *S. tokodaii* Sua5 (Agari et al., 2008). The function of YrdC-like proteins appears to be associated with RNA modifications. Crystallographic and nucleic acid-binding studies of *E. coli* YrdC suggested that this protein might exert its function through binding a double-stranded RNA (Kaczanowska and Rydén-Aulin, 2005; Teplova et al., 2000), and the yeast YrdC-like protein was recently shown to be essential for translational regulation in yeasts through tRNA modification (El Yacoubi et al., 2009; Lin et al., 2010). The residues flanking the nucleotide-binding site in HypF, and which are conserved in the YrdC-like proteins, include Lys243, Arg245, Thr321 (mostly), Ser322, and Asn324. These residues contact the phosphates and ribose of ATP, as well as Val/Leu101, Ala/Ile251, Leu/Phe294, and Val/Ile363, which contact the adenine base. This residue pattern is not conserved in YciO, which may bind different ligands in this deep pocket.

The C-terminal domain of HypF also has structural homologs in the so-called universal proteins Kae1, present and essential in the three domains of life (Galperin and Koonin, 2004). The closest structural homologs are Kae1 from *Pyrococcus abyssi* (PDB ID codes 2IVN and 2IVP; Hecker et al., 2007), Kae1 from *Methanocaldococcus jannaschii* (PDB ID code 2VWB; Hecker et al., 2008), and the Kae1 component of the KEOPS complex from *Thermoplasma acidophilum* (PDB ID code 3ENO; Mao et al., 2008). They superimpose on HypF with an rmsd of ~1.6–1.7 Å for ~160 Cα atoms. These proteins were initially annotated as endopeptidases (Abdullah et al., 1992), but their actual function has been questioned (Galperin and Koonin, 2004). Kae1 from *P. abyssi* (PDB ID code 2IVP) was shown to be an iron-protein that binds ATP and both single- and double-stranded DNA (Hecker et al., 2007). The ATP in Kae1 binds in the same place as ADP in the C-terminal domain of HypF. Of the four residues that coordinate Zn^{2+} in HypF, His475, His479, and Asp727 are conserved in Kae1 whereas the fourth residue (Asp502) is replaced by a Tyr residue (Hecker et al., 2007). In archaeal *M. jannaschii* Kae1, a metal ion assigned as Mg^{2+} occupies a similar position as the Zn and the Fe atoms in other homologs.

Mechanistic Implications

The two nucleotide-binding sites are located at opposite sides of a large cavity at the interface between the middle and C-terminal domains and are separated by only ~14 Å. It appears that only site 1 (YrdC-like middle domain) can accommodate ATP, whereas site 2 (Kae1-like C-terminal domain) can receive only AMP or, at most, ADP. This arrangement suggests a channeling of a reaction intermediate from site 1 to site 2. Our observation of a carbamoyl adenylate intermediate in site 1 upon soaking the HypF(92–750) crystal with ATP and carbamoylphosphate argues that this reaction step occurs at site 1 and that the N-terminal (1–91) phosphatase domain is not required for this reaction. We hypothesize that the carbamoyl adenylate migrates subsequently to site 2 (C-terminal domain) before delivery of the carbamoyl group to HypE (Reissmann et al., 2003). According to the previous proposal (Paschos et al., 2002), formation of the carbamoyl adenylate is associated with a release of PP_i and P_i. The presence of a tunnel under the ATP α-phosphate in site 1 suggests that this is the binding site for the carbamoylphosphate or carbamate substrate and would indicate an ordered reaction with this substrate binding first, followed by ATP binding. Interestingly, our experiments with the full-length mutants that affected ATP/ADP binding in sites 1 or 2 showed that the carbamoylphosphate phosphatase activity was retained in the absence of the nucleotide. This is probably possible because carbamoylphosphate hydrolyzes readily, and it just needs to be "trapped" in the reaction chamber and it will eventually hydrolyze. Having an ATP molecule there leads to the formation of the carbamoyl adenylate product. The addition of an acylphosphatase module might make this much more efficient and competitive, with the consequence that hydrogenase maturation

can compete with arginine and pyrimidine biosynthesis for the carbamoylphosphate substrate. This would also explain the "tunnel" emerging behind the carbamoyl adenylate-binding site and is the possible structural function of the zinc-finger motif. The formation of carbamoyl adenylate is essentially merely a means of stabilizing the carbamate moiety until it can react with the enzyme's "true" substrate—the cysteinyl residue of HypE. Notably, some bacteria, for example *Ralstonia eutropha* H16, have a truncated version of HypF that includes only the C-terminal domain (Wolf et al., 1998). Further copies of full-length HypF (HypF2 and HypF3) known to be present in these bacteria might, however, supply this truncated HypF1 derivative with the carbamoyl adenylate intermediate. Clearly, the detailed chemical steps of the overall carbamoyl transfer reaction are not yet clear, even with the knowledge of the crystal structure.

The N-terminal acylphosphatase domain, missing in the present structure, is connected to the rest of the protein by a long and flexible linker. This linker, residues 92–100, is disordered in the present structure. The length of this linker and its flexibility, also reflected in our inability to crystallize the full-length HypF, makes it difficult to predict the position of this domain relative to the rest of the protein. The acylphosphatase domain exhibits specificity for carbamoylphosphate (Paschos et al., 2002) in vitro, and it is essential for hydrogenase maturation activity of HypF in vivo.

EXPERIMENTAL PROCEDURES

Strains and Plasmid Construction

The strains used in this study were BL21(DE3) (F^- *ompT gal dcm lon* $hsdS_B(r_B^- m_B^-)$ λ*(DE3 lacI lacUV5-T7 gene 1 ind1 sam7 nin5)*) (Studier and Moffatt, 1986), MC4100 (F^-, *araD139*, Δ*(argF-lac)U169*, *ptsF25*, *deoC1*, *relA1*, *flbB5301*, *rspL150*, λ^-) (Casadaban and Cohen, 1979), and DHP-F2 (like MC4100 but Δ*hypF* amino acids 59–629) (Paschos et al., 2002).

The DNA sequences encoding full-length HypF (HypF-FL) and the HypF (92–750) truncated variant were amplified from *E. coli* O157:H7 EDL933 genomic DNA. The genes on the amplified DNA fragments were cloned in-frame in the vector pRL652 for expression of TEV-cleavable GST-tagged protein.

Introduction of amino acid substitutions to improve crystallizability and to modify the putative ATP-binding sites of HypF was performed by the QuikChange mutagenesis procedure (Stratagene) as described by the manufacturer and using a plasmid containing the 92–750 insert or full-length entire HypF gene as a template DNA with the oligonucleotide primers listed in Table S1 (available online). The resulting plasmids were named according to the amino acid substitution or substitutions introduced into the encoded HypF variant: pFG298M and pFK243Q/R245Q carry amino acid substitutions in the middle domain of HypF; and pFH475A/H479A, pFG697A, and pFG697V have substitutions in the C-terminal domain of HypF. Plasmid pZL364 carries a gene encoding a HypF(92–750) variant with the triple-substitution Q571A/Q572A/Q573A, referred to as HypFM3.

Expression of *hypF* and Purification of Recombinant Proteins

GST-HypF fusion protein variants were overproduced in *E. coli* BL21(DE3) cells. Cells containing the plasmids encoding HypF-FL and HypF(92–750) were grown aerobically at 37°C in 1 l of LB medium containing 100 μg/ml ampicillin to the mid-exponential phase, and protein overproduction was initiated by adding isopropyl-β-D-galactopyranoside to a final concentration of 0.2 mM. The temperature was reduced to 20°C and incubation was continued with shaking overnight. Cells were harvested by centrifugation (4,000 rpm, 30 min, 4°C), resuspended in a buffer consisting of 50 mM HEPES (pH 8.5) and 400 mM NaCl, and lysed on ice by sonication using alternating cycles of 10 s on/off for a total of 3 min. Following sonication, protease inhibitors (0.5 mM benzamidine and 0.01 mM leupeptin) as well as RNase and DNase (0.5 μg of each) were added to the lysate. The lysate was clarified by centrifugation (15,000 rpm, 4°C, 60 min) and the supernatant was removed. All purification steps were carried out aerobically. The protein was applied to a 2 ml bed volume of GST beads (GE Healthcare) pre-equilibrated with the sonication buffer. The mixture was incubated for 1 hr at room temperature, and then packed into a column and washed using gravity flow with 20 column volumes of the same buffer. The amount of protein retained on the beads was assessed using the Bradford assay. The GST tag was cleaved on the column by the addition of TEV protease (Kapust and Waugh, 2000) at a protease:protein ratio of 1:50 and incubating overnight at room temperature. The cleaved HypF protein was eluted from the column with the wash buffer, which was identical to the resuspension buffer. A 500 μl aliquot of HypF was then loaded onto a Superdex 200 column equilibrated with 20 mM HEPES (pH 8.5) and 200 mM NaCl. HypF-FL eluted from this column showed a dynamic equilibrium between dimers (apparent molecular mass of 190 kDa) and monomers (90 kDa). HypF(92–750) eluted from this column as a monomer with an apparent molecular mass of 70 kDa. Protein purity was assessed by SDS-PAGE. All HypF proteins were concentrated to 6–8 mg/ml by ultrafiltration in a final buffer of 20 mM HEPES (pH 8.5) and 100 mM NaCl prior to crystallization.

Crystallization

Initial crystallization trials with HypF(92–750) were performed by the sitting-drop vapor-diffusion method in Intelli-Plates (Art Robbins) using 0.4 μl protein and 0.4 μl reservoir solution and JCSG+, Classic I and II (QIAGEN) screens. No crystals were obtained initially. To improve the chances of crystallization by reducing surface entropy (Cooper et al., 2007), three consecutive glutamine residues in the HypF(92–750) construct were mutated to alanines resulting in a HypFM3 Q571A/Q572A/Q573A triple mutant. This protein led to crystals grown from mother liquor containing 22% (w/v) polyacrylic acid 5100 sodium salt, 0.1 M HEPES (pH 8.5), and 20 mM $MgCl_2$. Initial crystals appeared as clusters of needles and were optimized to yield separate chunky bars under the final crystallization condition: 26% (w/v) polyacrylic acid 5100 sodium salt, 0.1 M HEPES (pH 8.5), 20 mM $MgCl_2$, 2.5% (w/v) isopropanol, and 10% (w/v) ethylene glycol. The obtained crystals belong to the orthorhombic space group $P2_12_12_1$ with a = 46.3, b = 77.7, c = 199.9 Å, contain one molecule in the asymmetric unit with V_m = 2.51 $Å^3$/Da, and diffract to 2 Å resolution.

The SeMet-derivatized protein was prone to aggregation and did not crystallize. Instead, the heavy-atom derivative approach was pursued. Crystals of HypF were soaked in 10 mM $IrCl_3$ for 3 hr, and the iridium derivative diffracted to 3 Å resolution with only slightly different cell dimensions: a = 46.4, b = 78.2, c = 200.7 Å. The substrate-binding site was probed by overnight soaking of the HypF crystals with 5 mM carbamoylphosphate in combination with 5 mM ATP, AMP-CPP, AMP-PNP, ADP, or AMP.

Data Collection and Structure Determination

Diffraction data were collected at the CMCF1 beamline at the Canadian Light Source using a Mar300 CCD detector. Data integration and scaling were performed with HKL2000 (Otwinowski and Minor, 1997). The diffraction limits, crystal space group, and unit cell dimensions of the obtained crystals are presented in Table 2. The heavy-atom sites and the initial phases were obtained by the multiple isomorphous replacement with anomalous scattering method, with the native and two derivative data sets (Zn^{2+} and Ir^{3+}) collected at their respective absorption edges (1.28248 Å and 1.10498 Å) using the program autoSharp (Vonrhein et al., 2007). The initial model was built using RESOLVE software (Terwilliger, 2003) and finalized by application of alternating cycles of refinement using REFMAC5 (Winn et al., 2003) and refitting using Coot (Emsley and Cowtan, 2004). The final refinement cycles including the TLS parameters with HypFM3 divided into three groups. Data collection and refinement statistics are summarized in Table 2. In the structure of the HypFM3-AMP-PNP complex, one molecule of HypF is less well ordered for residues 118–124, 144–182, and 335–344, which likely leads to somewhat higher R factors.

The final model consists of residues 101–746. The nine N-terminal and six C-terminal residues are disordered and could not be reliably modeled. Coordinates and structure factors for apo-HypFM3, HypFM3-carbamoyl adenylate,

Table 2. Data Collection and Refinement Statistics

	Native	Ir Peak	Zn Peak	ATP+CP Fe Peak	ATP+CP Zn Peak	AMP-PNP+CP	ADP+CP	AMP-CPP+CP	AMP+CP
Data Collection									
Symmetry	$P2_12_12_1$	$P2_12_12_1$	$P2_12_12_1$	$P2_12_12_1$	$P2_12_12_1$	$P2_12_12_1$	$P2_12_12_1$	$P2_12_12_1$	$P2_12_12_1$
Wavelength (Å)	0.97949	1.10498	1.28248	1.73989	1.28248	0.97949	0.97949	0.97949	0.97949
a	46.3	46.4	46.6	46.5	46.5	46.3	46.4	46.4	46.4
b	77.7	78.2	77.5	78.1	78.3	75.0	77.9	77.7	75.6
c (Å)	199.9	200.7	200.6	200.4	200.8	201.3	200.5	200.6	200.7
Number of reflections	169,629	86,999	265,256	76,635	95,601	256,814	387,673	161,878	186,262
Number of unique reflections	46,522	18,652	44,061	29,433	29,549	54,251	62,057	37,601	50,071
Resolution	50–2.05 (2.09–2.05)	50–2.8 (2.85–2.8)	50–2.09 (2.13–2.09)	50–2.4 (2.44–2.4)	50–2.4 (2.44–2.4)	50–1.92 (1.95–1.92)	50–1.86 (1.89–1.86)	50–2.20 (2.24–2.20)	50–1.92 (1.95–1.92)
Redundancy	3.8 (2.6)	4.8 (4.1)	6.2 (3.1)	3.2 (3.0)	3.5 (3.2)	5.6 (4.2)	6.3 (4.8)	4.6 (4.6)	3.7 (3.2)
Completeness (%)	92.5 (62.0)	97.7 (92.4)	93.9 (63.7)	82.5 (71.4)	92.0 (82.7)	85.2 (80.3)	99.4 (96.2)	94.6 (87.1)	90.6 (80.1)
$\langle I/\sigma(I)\rangle$	16.7 (4.1)	38.1 (15.2)	18.7 (2.2)	35.1 (11.3)	33.9 (11.3)	21.8 (1.7)	38.8 (6.9)	39.6 (13.2)	27.1 (2.7)
R_{sym}[a]	0.063	0.05	0.112	0.104	0.041	0.094	0.066	0.053	0.05
Overall B (Å^2)	17.7	39.7	26.7	31.9	29.8	24.4	15.0	21.6	21.3
Model Refinement									
Number of protein atoms	4,945				4,934	4,938	5,051	4,969	4,929
Number of solvent atoms	644				414	602	719	341	447
Number of ions	4				4	4	4	4	4
R_{cryst}[a]	0.159				0.154	0.203	0.159	0.162	0.177
R_{free}	0.206				0.233	0.259	0.202	0.214	0.225
Geometry									
Rms bonds (Å)	0.016				0.021	0.018	0.013	0.019	0.016
Rms angles (°)	1.57				1.85	1.83	1.39	1.67	1.65
PDB ID code	3TSP				3TSQ	3TSU	3TTC	3TTD	3TTF

[a] $R_{merge} = \Sigma_{hkl}\,\Sigma_i|I_i(hkl) - \langle I(hkl)\rangle|/\Sigma_{hkl}\,\Sigma_i I_i(hkl)$, where Σ_{hkl} denotes the sum over all reflections and Σ_I is the sum over all equivalent and symmetry-related reflections.

HypFM3-AMP-PNP, HypFM3-ADP, HypFM3-AMP-CPP, and HypF-AMP have been deposited in the PDB under ID codes 3TSP, 3TSQ, 3TSU, 3TTC, 3TTD, and 3TTF, respectively.

Calorimetric Measurements

Samples were prepared in 20 mM HEPES (pH 7.5) and 200 mM sodium chloride. The concentration of HypF was determined spectrophotometrically at 280 nm using the theoretical extinction coefficient of 93,735 M^{-1} cm^{-1}. Concentrations of AMP-PNP and ADP were determined spectrophotometrically at 260 nm using the theoretical extinction coefficient of 15,400 M^{-1} cm^{-1}. All experiments were performed on an iTC200 microcalorimeter (MicroCal) at 20°C. The titrations were started with an initial injection of 0.8 μl and a second 3.2 μl injection, followed by nine 4 μl injections. The cell contained 400 μl of 70 μM HypF and the syringe contained 70 μl of 2 mM titrant solution. For all experiments, the first injection was removed and the heat of dilution integrals were subtracted prior to analysis with the instrument software.

Determination of Hydrogenase and Formate Hydrogenlyase Enzyme Activities

The activity of all three hydrogenases can be determined simultaneously in the H_2 oxidation direction by using the artificial electron acceptor benzyl viologen (BV) (Ballantine and Boxer, 1985). The total hydrogenase enzyme activity was determined as described previously (Ballantine and Boxer, 1985), except that the buffer used was 50 mM MOPS (pH 7.0). The wavelength used was 578 nm, and an extinction coefficient of 8,600 M^{-1} cm^{-1} was assumed for reduced BV. One unit of activity corresponded to the reduction of 1 μmol of hydrogen/min. Experiments were performed at least three times and each time in triplicate. Data are presented as standard deviation of the mean.

Quantitative determination of formate hydrogenlyase activity (dihydrogen evolution), which represents the activity of Hyd-3 only, was performed as described (Pinske and Sawers, 2010). Briefly, cultures were grown in LB medium containing 0.8% (w/v) glucose to an OD_{600nm} of 0.6, and 10 ml of culture was harvested by centrifugation and resuspended in 1 ml of 50 mM MOPS buffer (pH 7.0) and placed in a Hungate tube under an N_2 atmosphere. Aliquots of 200 μl of cells were withdrawn and introduced into a fresh small Hungate tube. The reaction was started by adding 20 μl of 3 M sodium formate, and 200 μl of the gas phase was analyzed at six time points between 3 and 18 min by gas chromatography (GC4000; Fisons Instruments) with molecular sieve column 5A, 80/100 mesh. Pure nitrogen was used as the carrier gas. The amount of dihydrogen gas produced per unit time was calculated based on a standard curve using defined concentrations of dihydrogen gas. From the initial velocities the specific activities were calculated and are given in mU/mg of protein.

In-Gel Staining for Hydrogenase Enzyme Activity

Nondenaturating PAGE was performed using 5% (w/v) polyacrylamide gels (pH 8.5) and containing 0.1% (w/v) Triton X-100 (Ballantine and Boxer, 1985). Samples of crude extract (25 μg of protein) were incubated with 5% (w/v) Triton X-100 prior to application on the gels. Hydrogenase activity staining was done as described in Ballantine and Boxer (1985), except that the buffer used was 50 mM MOPS (pH 7.0).

Small-Scale Purification of His-Tagged HypF Variants and Determination of In-Gel Carbamoylphosphate Phosphatase Activity

Small amounts of His-tagged HypF variants with amino acid substitutions in the ATP-binding sites were purified anaerobically following Soboh et al. (2010). Briefly, 60 mg of crude cell extract (3–5 ml) in buffer A (50 mM Tris/HCl [pH 8] and 300 mM NaCl) was loaded onto 0.5 ml TALON Superflow Matrix resin preloaded with cobalt ions and washed with a minimum of five column volumes of buffer A. Two further wash steps were applied in which 5 mM and then 10 mM imidazole was included in buffer A. Finally, the bound HypF proteins were eluted by applying buffer A containing 300 mM imadazole. The elution fractions (500 μl) containing HypF were concentrated to 20 μl using Vivaspin 6 concentrators (Sartorius Stedim). Aliquots (10 μl) were applied either to 10% (w/v) SDS-PAGE or 5% (w/v) native PAGE. After electrophoretic separation of overproduced HypF proteins by native PAGE, the carbamoylphosphate phosphatase activity was determined directly in the gel by measuring the release of inorganic phosphate exactly as described (Mizuno et al., 1989).

SUPPLEMENTAL INFORMATION

Supplemental Information includes one table and can be found with this article online at doi:10.1016/j.str.2011.09.023.

ACKNOWLEDGMENTS

The data collection described in this paper was performed at the Canadian Light Source, which is supported by NSERC, NRC, CIHR, and the University of Saskatchewan. This work was supported by grant GSP-48370 from the Canadian Institutes of Health Research (to M.C.). We would like to thank Mr. S. Labiuk for help with data collection. We also thank Dr. Guennadi Kozlov for help with ITC experiments, Dr. Milton Stubbs for his input and suggestions regarding the carbamoyl adenylate in the HypF structure, and Dr. Allan Matte for helpful suggestions and comments on the manuscript. This research was supported by CIHR grant GSP-48370 (to M.C.) and the Deutsche Forschungsgemeinschaft (SA 494/3-1) and MLU Halle (to R.G.S.).

Received: July 31, 2011
Revised: September 13, 2011
Accepted: September 22, 2011
Published: December 6, 2011

REFERENCES

Abdullah, K.M., Udoh, E.A., Shewen, P.E., and Mellors, A. (1992). A neutral glycoprotease of *Pasteurella haemolytica* A1 specifically cleaves O-sialoglycoproteins. Infect. Immun. *60*, 56–62.

Agari, Y., Sato, S., Wakamatsu, T., Bessho, Y., Ebihara, A., Yokoyama, S., Kuramitsu, S., and Shinkai, A. (2008). X-ray crystal structure of a hypothetical Sua5 protein from *Sulfolobus tokodaii* strain 7. Proteins *70*, 1108–1111.

Ballantine, S.P., and Boxer, D.H. (1985). Nickel-containing hydrogenase isoenzymes from anaerobically grown *Escherichia coli* K-12. J. Bacteriol. *163*, 454–459.

Blokesch, M., Rohrmoser, M., Rode, S., and Böck, A. (2004a). HybF, a zinc-containing protein involved in NiFe hydrogenase maturation. J. Bacteriol. *186*, 2603–2611.

Blokesch, M., Paschos, A., Bauer, A., Reissmann, S., Drapal, N., and Böck, A. (2004b). Analysis of the transcarbamoylation-dehydration reaction catalyzed by the hydrogenase maturation proteins HypF and HypE. Eur. J. Biochem. *271*, 3428–3436.

Böck, A., King, P.W., Blokesch, M., and Posewitz, M.C. (2006). Maturation of hydrogenases. Adv. Microb. Physiol. *51*, 1–71.

Casadaban, M.J., and Cohen, S.N. (1979). Lactose genes fused to exogenous promoters in one step using a Mu-lac bacteriophage: in vivo probe for transcriptional control sequences. Proc. Natl. Acad. Sci. USA *76*, 4530–4533.

Cooper, D.R., Boczek, T., Grelewska, K., Pinkowska, M., Sikorska, M., Zawadzki, M., and Derewenda, Z. (2007). Protein crystallization by surface entropy reduction: optimization of the SER strategy. Acta Crystallogr. D Biol. Crystallogr. *63*, 636–645.

El Yacoubi, B., Lyons, B., Cruz, Y., Reddy, R., Nordin, B., Agnelli, F., Williamson, J.R., Schimmel, P., Swairjo, M.A., and de Crécy-Lagard, V. (2009). The universal YrdC/Sua5 family is required for the formation of threonylcarbamoyladenosine in tRNA. Nucleic Acids Res. *37*, 2894–2909.

Emsley, P., and Cowtan, K. (2004). Coot: model-building tools for molecular graphics. Acta Crystallogr. D Biol. Crystallogr. *60*, 2126–2132.

Forzi, L., and Sawers, R.G. (2007). Maturation of [NiFe]-hydrogenases in *Escherichia coli*. Biometals *20*, 565–578.

Galperin, M.Y., and Koonin, E.V. (2004). 'Conserved hypothetical' proteins: prioritization of targets for experimental study. Nucleic Acids Res. *32*, 5452–5463.

Gasper, R., Scrima, A., and Wittinghofer, A. (2006). Structural insights into HypB, a GTP-binding protein that regulates metal binding. J. Biol. Chem. *281*, 27492–27502.

Harding, M.M. (2006). Small revisions to predicted distances around metal sites in proteins. Acta Crystallogr. D Biol. Crystallogr. *62*, 678–682.

Hecker, A., Leulliot, N., Gadelle, D., Graille, M., Justome, A., Dorlet, P., Brochier, C., Quevillon-Cheruel, S., Le Cam, E., van Tilbeurgh, H., and Forterre, P. (2007). An archaeal orthologue of the universal protein Kae1 is an iron metalloprotein which exhibits atypical DNA-binding properties and apurinic-endonuclease activity in vitro. Nucleic Acids Res. *35*, 6042–6051.

Hecker, A., Lopreiato, R., Graille, M., Collinet, B., Forterre, P., Libri, D., and van Tilbeurgh, H. (2008). Structure of the archaeal Kae1/Bud32 fusion protein MJ1130: a model for the eukaryotic EKC/KEOPS subcomplex. EMBO J. *27*, 2340–2351.

Holm, L., Kääriäinen, S., Rosenström, P., and Schenkel, A. (2008). Searching protein structure databases with DaliLite v.3. Bioinformatics *24*, 2780–2781.

Jia, J., Lunin, V.V., Sauve, V., Huang, L.W., Matte, A., and Cygler, M. (2002). Crystal structure of the YciO protein from *Escherichia coli*. Proteins *49*, 139–141.

Kaczanowska, M., and Rydén-Aulin, M. (2005). The YrdC protein—a putative ribosome maturation factor. Biochim. Biophys. Acta *1727*, 87–96.

Kapust, R.B., and Waugh, D.S. (2000). Controlled intracellular processing of fusion proteins by TEV protease. Protein Expr. Purif. *19*, 312–318.

Lin, C.A., Ellis, S.R., and True, H.L. (2010). The Sua5 protein is essential for normal translational regulation in yeast. Mol. Cell. Biol. *30*, 354–363.

Mao, D.Y., Neculai, D., Downey, M., Orlicky, S., Haffani, Y.Z., Ceccarelli, D.F., Ho, J.S., Szilard, R.K., Zhang, W., Ho, C.S., et al. (2008). Atomic structure of the KEOPS complex: an ancient protein kinase-containing molecular machine. Mol. Cell *32*, 259–275.

Mehta, N., Olson, J.W., and Maier, R.J. (2003). Characterization of *Helicobacter pylori* nickel metabolism accessory proteins needed for maturation of both urease and hydrogenase. J. Bacteriol. *185*, 726–734.

Mizuno, Y., Ohba, Y., Fujita, H., Kanesaka, Y., Tamura, T., and Shiokawa, H. (1989). Activity staining of acylphosphatase after gel electrophoresis. Anal. Biochem. *183*, 46–49.

Mulder, D.W., Boyd, E.S., Sarma, R., Lange, R.K., Endrizzi, J.A., Broderick, J.B., and Peters, J.W. (2010). Stepwise [FeFe]-hydrogenase H-cluster assembly revealed in the structure of HydA(DeltaEFG). Nature *465*, 248–251.

Otwinowski, Z., and Minor, W. (1997). Processing of X-ray diffraction data collected in oscillation mode. Methods Enzymol. *276*, 307–326.

Paschos, A., Bauer, A., Zimmermann, A., Zehelein, E., and Böck, A. (2002). HypF, a carbamoyl phosphate-converting enzyme involved in [NiFe] hydrogenase maturation. J. Biol. Chem. *277*, 49945–49951.

Peters, J.W., Lanzilotta, W.N., Lemon, B.J., and Seefeldt, L.C. (1998). X-ray crystal structure of the Fe-only hydrogenase (CpI) from *Clostridium pasteurianum* to 1.8 angstrom resolution. Science *282*, 1853–1858.

Pinske, C., and Sawers, R.G. (2010). The role of the ferric-uptake regulator Fur and iron homeostasis in controlling levels of the [NiFe]-hydrogenases in *Escherichia coli*. Int. J. Hydrogen Energy *35*, 8938–8944.

Rangarajan, E.S., Asinas, A., Proteau, A., Munger, C., Baardsnes, J., Iannuzzi, P., Matte, A., and Cygler, M. (2008). Structure of [NiFe] hydrogenase maturation protein HypE from *Escherichia coli* and its interaction with HypF. J. Bacteriol. *190*, 1447–1458.

Reissmann, S., Hochleitner, E., Wang, H., Paschos, A., Lottspeich, F., Glass, R.S., and Böck, A. (2003). Taming of a poison: biosynthesis of the NiFe-hydrogenase cyanide ligands. Science *299*, 1067–1070.

Rosano, C., Zuccotti, S., Bucciantini, M., Stefani, M., Ramponi, G., and Bolognesi, M. (2002). Crystal structure and anion binding in the prokaryotic hydrogenase maturation factor HypF acylphosphatase-like domain. J. Mol. Biol. *321*, 785–796.

Shomura, Y., Komori, H., Miyabe, N., Tomiyama, M., Shibata, N., and Higuchi, Y. (2007). Crystal structures of hydrogenase maturation protein HypE in the Apo and ATP-bound forms. J. Mol. Biol. *372*, 1045–1054.

Soboh, B., Krüger, S., Kuhns, M., Pinske, C., Lehmann, A., and Sawers, R.G. (2010). Development of a cell-free system reveals an oxygen-labile step in the maturation of [NiFe]-hydrogenase 2 of *Escherichia coli*. FEBS Lett. *584*, 4109–4114.

Studier, F.W., and Moffatt, B.A. (1986). Use of bacteriophage T7 RNA polymerase to direct selective high-level expression of cloned genes. J. Mol. Biol. *189*, 113–130.

Teplova, M., Tereshko, V., Sanishvili, R., Joachimiak, A., Bushueva, T., Anderson, W.F., and Egli, M. (2000). The structure of the yrdC gene product from *Escherichia coli* reveals a new fold and suggests a role in RNA binding. Protein Sci. *9*, 2557–2566.

Terwilliger, T.C. (2003). Automated main-chain model building by template matching and iterative fragment extension. Acta Crystallogr. D Biol. Crystallogr. *59*, 38–44.

Thauer, R.K., Kaster, A.K., Goenrich, M., Schick, M., Hiromoto, T., and Shima, S. (2010). Hydrogenases from methanogenic archaea, nickel, a novel cofactor, and H_2 storage. Annu. Rev. Biochem. *79*, 507–536.

Vignais, P.M., and Billoud, B. (2007). Occurrence, classification, and biological function of hydrogenases: an overview. Chem. Rev. *107*, 4206–4272.

Volbeda, A., Charon, M.H., Piras, C., Hatchikian, E.C., Frey, M., and Fontecilla-Camps, J.C. (1995). Crystal structure of the nickel-iron hydrogenase from *Desulfovibrio gigas*. Nature *373*, 580–587.

Vonrhein, C., Blanc, E., Roversi, P., and Bricogne, G. (2007). Automated structure solution with autoSHARP. Methods Mol. Biol. *364*, 215–230.

Wang, L., Xia, B., and Jin, C. (2007). Solution structure of *Escherichia coli* HypC. Biochem. Biophys. Res. Commun. *361*, 665–669.

Watanabe, S., Matsumi, R., Arai, T., Atomi, H., Imanaka, T., and Miki, K. (2007). Crystal structures of [NiFe] hydrogenase maturation proteins HypC, HypD, and HypE: insights into cyanation reaction by thiol redox signaling. Mol. Cell *27*, 29–40.

Watanabe, S., Arai, T., Matsumi, R., Atomi, H., Imanaka, T., and Miki, K. (2009). Crystal structure of HypA, a nickel-binding metallochaperone for [NiFe] hydrogenase maturation. J. Mol. Biol. *394*, 448–459.

Winn, M.D., Murshudov, G.N., and Papiz, M.Z. (2003). Macromolecular TLS refinement in REFMAC at moderate resolutions. Methods Enzymol. *374*, 300–321.

Wolf, I., Buhrke, T., Dernedde, J., Pohlmann, A., and Friedrich, B. (1998). Duplication of hyp genes involved in maturation of [NiFe] hydrogenases in *Alcaligenes eutrophus* H16. Arch. Microbiol. *170*, 451–459.

Xia, W., Li, H., Sze, K.H., and Sun, H. (2009). Structure of a nickel chaperone, HypA, from *Helicobacter pylori* reveals two distinct metal binding sites. J. Am. Chem. Soc. *131*, 10031–10040.